Electrochimica Acta 109 (2013) 291–297

Contents lists available at ScienceDirect

Electrochimica Acta

journal homepage: www.elsevier.com/locate/electacta

Enhanced performance of dye/QDs cosensitized solar cells via Förster resonance energy transfer

Donglai Han[a,b], Yunfei Sun[a,b], Jinghai Yang[c,d,*], Lili Yang[c,d], Sihan Jin[c,d], Gang Chen[c,d], Hang Song[a]

[a] State Key Laboratory of Luminescence and Applications, Changchun Institute of Optics, Fine Mechanics and Physics, Chinese Academy of Sciences, Changchun 130033, China
[b] University of Chinese Academy of Sciences, Beijing 100049, China
[c] Institute of Condensed State Physics, Jilin Normal University, Siping 136000, China
[d] Key Laboratory of Functional Materials Physics and Chemistry of the Ministry of Education, Jilin Normal University, Siping 136000, Jilin, China

ARTICLE INFO

Article history:
Received 15 May 2013
Received in revised form 11 July 2013
Accepted 11 July 2013
Available online 26 July 2013

Keywords:
ZnO/ZnS photoanode
Light absorbance
QDSSCs
Cosensitized solar cells

ABSTRACT

In this report, CdS quantum dots (QDs) and N719/QDs cosensitized solar cells with ZnO/ZnS hierarchical structures as photoanodes are constructed. The ZnO/ZnS hierarchical structures consist of highly oriented ZnO nanorod arrays coated with ZnS nanoparticles (NPs), this construction is efficient on retarding the back transfer of electrons and inhibiting the recombination of electrons at the anode/sensitizers/electrolyte interfaces. The influence of deposition time for CdS QDs on photovoltaic performance of the ZnO/ZnS/CdS electrodes is explored and optimized photovoltaic performance is obtained from the device based on ZnO/ZnS/CdS(12) electrode, with a *Voc* of 0.66 V, a *Jsc* of 3.66 mA/cm^2, an *FF* of 0.48, and a η of 1.16%. The cosensitized solar cell exhibits a 37% enhancement in energy conversion efficiency compared with the device sensitized by CdS QDs only, which is attributed to the higher light absorbance of the cosensitized solar cells than that of CdS sensitized solar cells.

1. Introduction

Although the fossil fuels dominate the energy source market through the last century, the solar energy is considered as the cleanest and least limited energy source all along. The solar cell is a device that can convert the energy of sunlight into electric energy. Among all types of solar cells, a new generation solar cells using dyes or quantum dots (QDs) as sensitizer have recently attracted a lot interest due to their low cost and simple fabrication processes [1–5]. However, both dyes and QDs still face several problems. For example, Quintana et al. and Ganesh et al. reported that the acidic ruthenium dye will degrade under full sun irradiation and lead to the formation of Zn^{2+}/dye complex, i.e. a relatively nonconductive/insulating layer, which generally blocks the overall electron injection efficiency of the dye molecules and results in the inferior device conversion efficiency [6,7]. Of course, QDs also have their disadvantage. The efficient charge separation and fast charge transport are their major challenges [8,9].

So far, a lot of effort has been made to overcome the above disadvantages and improve the performance of both QDs and dye sensitized solar cells [10–12]. Among them, the QDs and dye cosensitizing are a burgeoning approach. On one hand, as Buhbut et al. reported about dye-sensitized solar cells, the incorporation of inorganic semiconductor QDs into the solid titania electrode resulted in high energy transfer efficiency and significant improvement of the cell stability. On the other hand, the light absorption will be enhanced and absorption spectrum will be broadened by the addition of QDs acting as “antennas”, which effectively increases the number of photons harvested by the dye sensitized solar cell and finally leads to the good performance [13]. Förster resonance energy transfer (FRET) is identified as electronic energy transfer, which has recently experienced a lot of research interest [11]. FRET has been used in solar concentrators [14] and to improve quantum yields in organic light-emitting devices [15,16]. Several ideas for FRET-based photovoltaic device enhancement have been proposed, for example Etgar et al. demonstrated that an enhancement of the cell photovoltaic parameters in CdSe QDs/VG1-C10 dye cosensitized solar cell was mainly ascribed to the FRET [17]. In addition, CdS QDs can hinder the contact of ZnS and N719 to form Zn^{2+}/dye complex. So, the concept of cosensitization is very significant in the new generation solar cells. For ZnO based solar cell, dots/N3 dual photosensitization improve the solar-to-electrical conversion efficiency due to the effective coupling between ZnO NPs/N3 dye molecules in the presence of CdS QDs [7]. On one hand, there is no report on QDs and N719 cosensitized solar cells; On the other hand,

* Corresponding author at: Institute of Condensed State Physics, Jilin Normal University, Siping 136000, China. Tel.: +86 434 3294566; fax: +86 434 3294566.
E-mail address: jhyang1@jlnu.edu.cn (J. Yang).

0013-4686/$ – see front matter © 2013 Elsevier Ltd. All rights reserved.
http://dx.doi.org/10.1016/j.electacta.2013.07.090

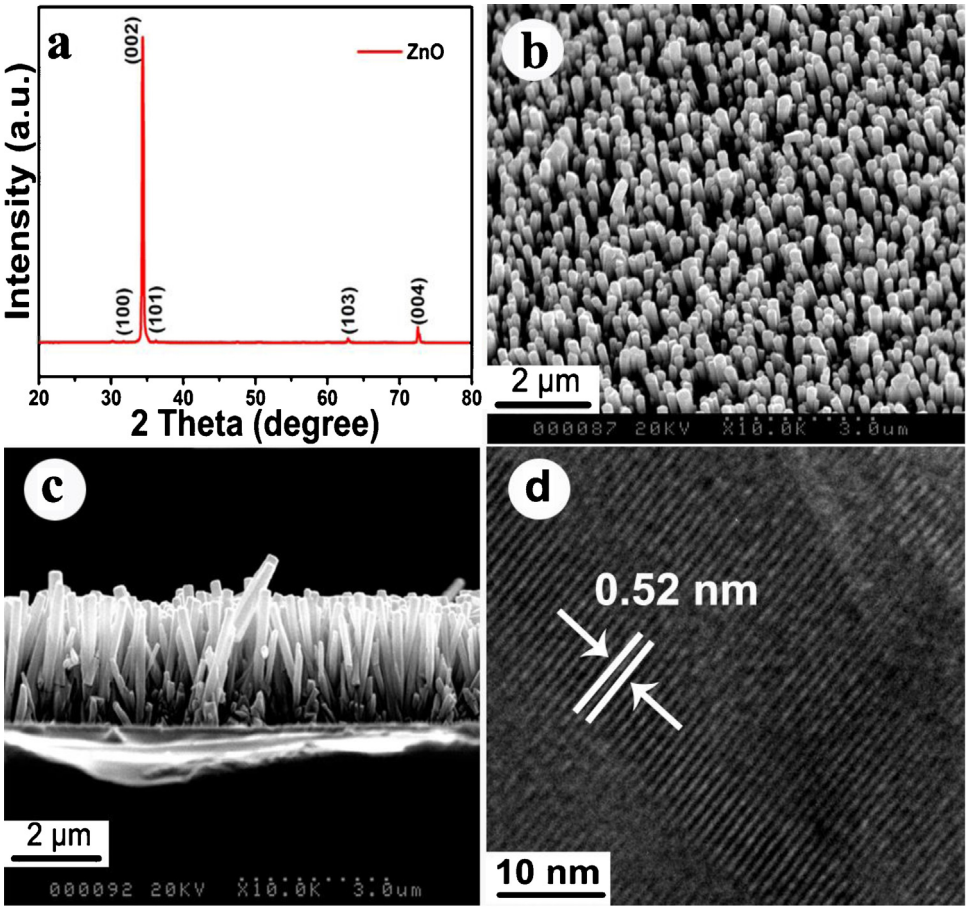

Fig. 1. (a) XRD pattern, (b) SEM (tilted view) image, (c) cross-sectional view and (d) HRTEM image of ZnO NRs.

the enhancement mechanism of cosensitized solar cells is not very clear and needs further investigation.

Inspired by these incentives, ZnO/ZnS heterostructure is used as photoanode since the compact ZnS shell is very efficient on retarding the back transfer of electrons and minimizing electron–hole recombination, which significantly decreases the dark current and is beneficial for the final conversion efficiency [18]. The influences of deposition times for CdS and dipping time of N719 on the photovoltaic performance were investigated on the ZnO/ZnS electrodes. By using the light absorption curve, we have explored the performance enhancement mechanism for cosensitized solar cells with QDs and N719 dye as cosensitizers.

2. Experimental methods

ZnO nanorods (NRs) were grown on ITO substrates by a two-step chemical bath deposition (CBD) method. The synthesizing details of ZnO NRs can be found elsewhere in our previous work [19]. The ZnS layer was deposited by successive ionic layer adsorption and reaction (SILAR). ZnO NRs prepared by above method were immersed in a 0.1 M $Zn(NO_3)_2$ solution for 5 min. They were then rinsed with distilled water and immersed in a 0.1 M Na_2S solution for another 5 min followed by another rinsing with distilled water. The two-step dipping procedure is termed as one SILAR cycle. The SILAR cycle was repeated for 10 times. The substrates with ZnO/ZnS composite structures were annealed at 150 °C for 30 min. The CdS QDs were also deposited by successive ionic layer adsorption and reaction (SILAR). The ZnO/ZnS composite structures prepared by above method were immersed in a 0.1 M $Cd(NO_3)_2$ solution for 5 min. They were then rinsed with distilled water and immersed in a 0.1 M Na_2S solution for another 5 min followed by another rinsing with distilled water. This SILAR cycle was repeated for several times. Dye adsorption was carried out by immersing the photoanode in a 0.3 mM ethanol solution of N719 at room temperature for different times (12 h, 17 h and 24 h). The electrodes were sandwiched and bonded with a platinum-coated indium tin oxide (ITO) (20 nm thick) counter electrodes to construct QDSSCs. The photoanode and the counter electrode were separated by a 60 μm thick polypropylene spacer; an ethanol solution consisting of 0.5 M LiI and 0.05 M I_2 was used as electrolyte.

X-ray diffraction (XRD) patterns were recorded by a MAC Science MXP-18 X-ray diffractometer using a Cu target radiation source. X-ray photoelectron spectra (XPS) were recorded on a VG ESCALAB Mark II XPS using Mg $K\alpha$ radiation ($h\nu$ = 1253.6 eV) with a resolution of 1.0 eV. Scanning electron microscopy (SEM) pictures were collected on a Hitachi, S-570 SEM. Transmission electron micrographs (TEM) and high-resolution transmission electron microscopy (HRTEM) images were taken on JEM-2100 transmission electron microscope. The photocurrent dependence on the voltage (J–V) was measured under AM 1.5G simulated sunlight illumination (100 mW/cm^2, Model 91160, Oriel). The room temperature photoluminescence (PL) measurements were carried out on the Renishaw inVia micro-PL spectrometer. A continuous 325 nm light of a He–Cd laser was used as the excitation source. UV–vis absorption spectra were measured on an UV-5800PC spectrometer.

3. Results and discussion

Fig. 1(a) shows the XRD patterns of highly oriented ZnO NRs grown on ITO substrates. All the observed diffraction peaks can be

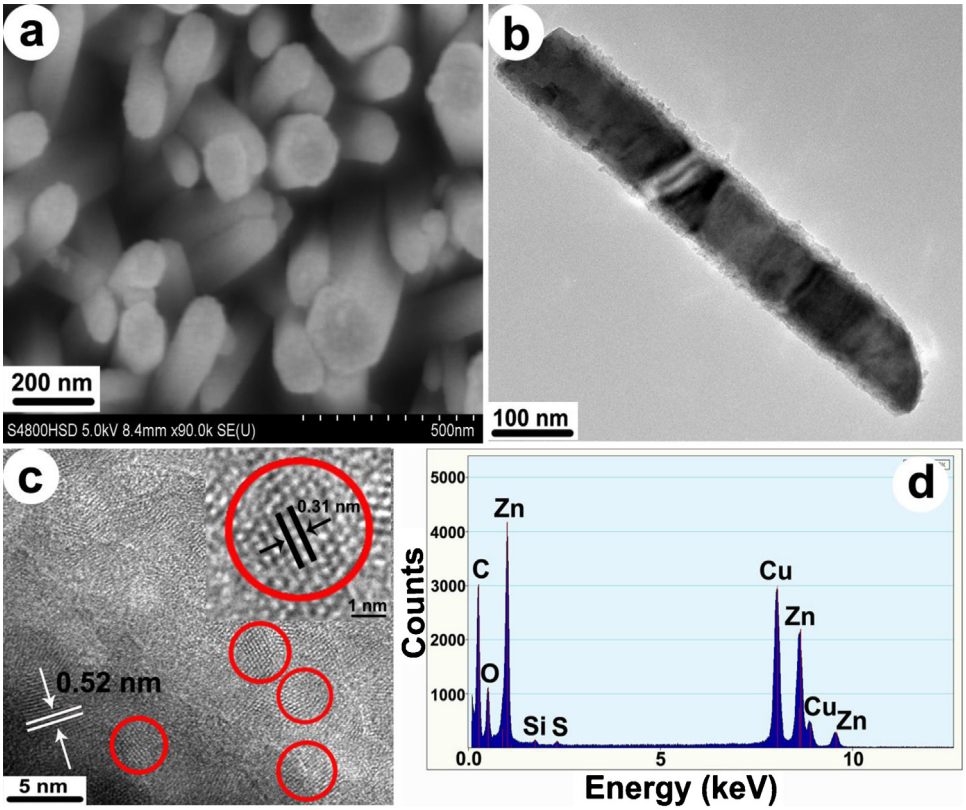

Fig. 2. (a) SEM (tilted view) image, (b) TEM image, (c) HRTEM image and (d) EDX spectra of NRs after ZnS deposition.

indexed to a wurtzite hexagonal-phase of pure ZnO (JCPDS card, No. 80-0074), which indicates no other impurity phase exists in the samples [20,21]. We can also notice that the intensity of the (0 0 2) diffraction peak is the strongest, which illustrates the highly preferential orientation of ZnO NRs arrays along *c*-axis [22]. The narrow FWHM (full width at half maximum) of the ZnO NRs indicates good crystallinity of the as-grown NRs [23]. Fig. 1(b) shows the SEM (tilted view) image of the as-grown ZnO NRs. We can see that the large-scale and vertically aligned ZnO NRs are uniformly grown with high density over the entire surface of the ITO substrate. Fig. 1(c) shows the cross-sectional view of ZnO NRs, which clearly shows that the ZnO NRs with smooth surface and 2.8 μm in length are grown vertically on the substrate. Fig. 1(d) shows a high-resolution TEM image of the ZnO NRs, in which the marked interplanar d spacing of 0.52 nm corresponds to the (0 0 0 1) lattice plane of hexagon wurtzite ZnO [24].

Fig. 2(a) and (b) shows the SEM and TEM images of ZnO NRs after ZnS deposition. The micrographs clearly show that the surface of the NRs became rough after coating ZnS NPs. Fig. 2(c) shows the HRTEM image of ZnO/ZnS hierarchical structure. In Fig. 2(c), two different well-resolved lattice fringe spacing can be distinguished. A lattice fringe of 0.52 nm corresponds to the wurtzite ZnO nanostructure [25]. Inset of Fig. 2(c) shows the enlarged HRTEM pattern of ZnS NPs with average diameter of ~5 nm, which is corresponding to the particle marked by the red circles in Fig. 2(c). The well-resolved lattice fringe spacing can be well distinguished to be 0.31 nm, which is corresponding to wurtzite ZnS [26]. Clearly, a thin layer of ZnS NPs has been uniformly attached on the surface of the ZnO NRs, and the contact between them is intimate. The detailed composition of the product was also characterized using energy-dispersive X-ray spectrometry (EDX). Fig. 2(d) shows the in situ EDX elemental analysis spectra of the product, which indicates that the product contains Zn, O and S (the Cu, C and Si signals come from the TEM grid). The EDX results further confirm that the product is composed of ZnO and ZnS. According to the above experiment results, we can conclude that ZnS NPs have been successfully deposited on the whole surface of the ZnO NRs. Hence, the entire ZnO NRs are converted into the ZnO/ZnS core–shell hierarchical structure in our experiment process.

We further perform the XPS measurement on the ZnO/ZnS/CdS structure to prove the existence of ZnS layer and CdS layer on ZnO NRs. Fig. 3 shows the XPS survey spectra from the sample, in which all of the peaks can be ascribed to Zn, O, S and Cd elements [27]. We would like to mention that, for all XPS spectrum in Fig. 3, the binding energies have been calibrated by taking the carbon C1s peak (285.0 eV) as reference. The high resolution scans of Zn2p, O1s, S2p and Cd3d peaks are shown in Fig. 3(b)–(e). The two peak structure in Zn2p spectrum arises from the spin–orbit interaction with the Zn2p3/2 peak position at 1022 eV and the Zn 2p1/2 at 1045 eV as shown in Fig. 2(b), which closely matches with the doublet binding energies and FWHM (1.8 eV) for the bulk ZnO [28]. Fig. 2(c) presents the O1s XPS spectrum of the sample. The peak centered at 531.3 eV is associated to the O^{2-} ion in the wurtzite structure surrounded by Zn atoms with their full complement of nearest-neighbor O^{2-} ions [29–31]. Fig. 2(d) presents the S2p XPS spectrum. The XPS binding energies of Zn2p at 1022 eV and the S2p at 161.2 eV apparently indicate that a ZnS compact layer was successfully synthesized on the ZnO NRs using the SILAR method [32]. Fig. 3(e) shows a narrow-range XPS scans for the Cd element. The two peak structure in Cd3d core level arises from the spin–orbit interaction with the Cd 3d5/2 peak position at 404.82 eV and the Cd 3d3/2 at 411.57 eV [27]. The XPS binding energies of Cd3d at 404.82 eV and the S2p at 161.2 eV are indicative of the CdS compounds.

Normalized photoluminescence (PL) spectra of ZnO NRs and ZnO/ZnS hierarchical structure are displayed in Fig. 4, which shows a weak UV emission around 378 nm and a deep level emission band

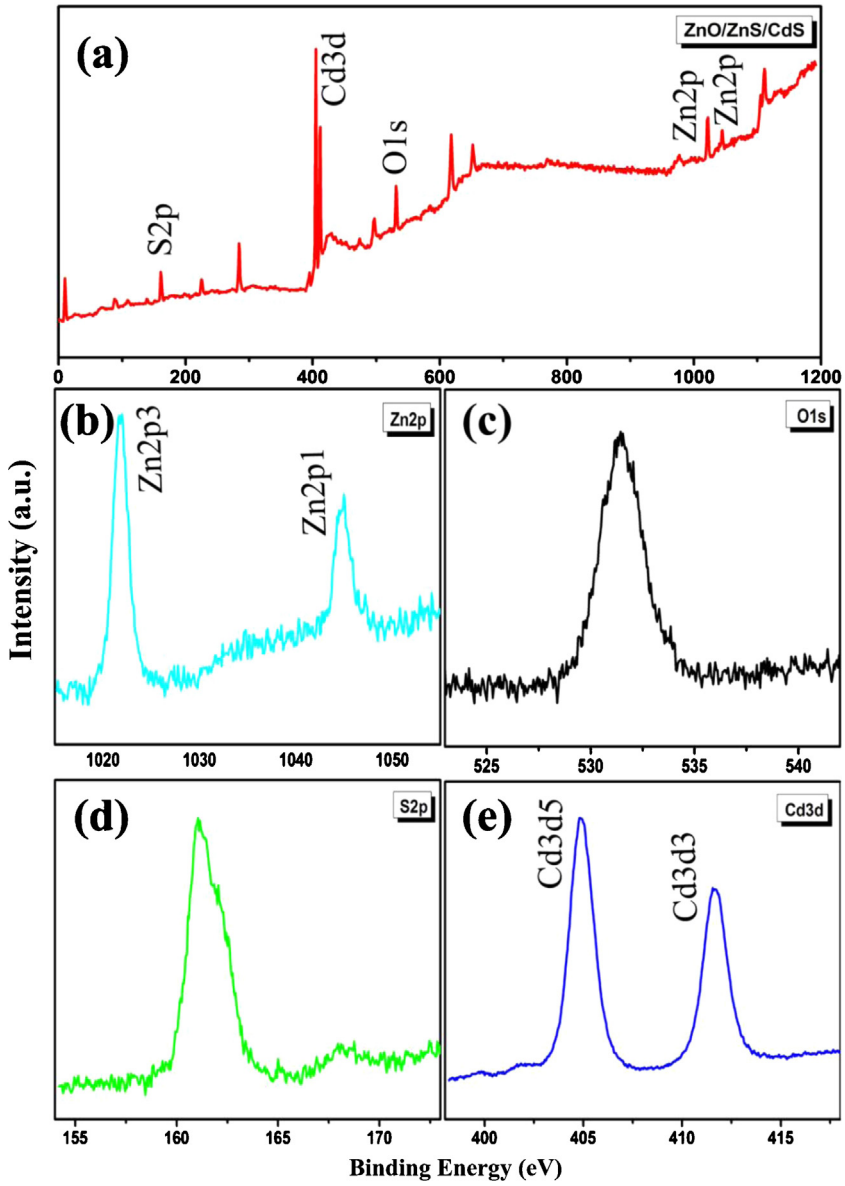

Fig. 3. (a) XPS analysis of ZnO/ZnS/CdS structure and (b–e) narrow range scans for the Zn, O, S and Cd, respectively.

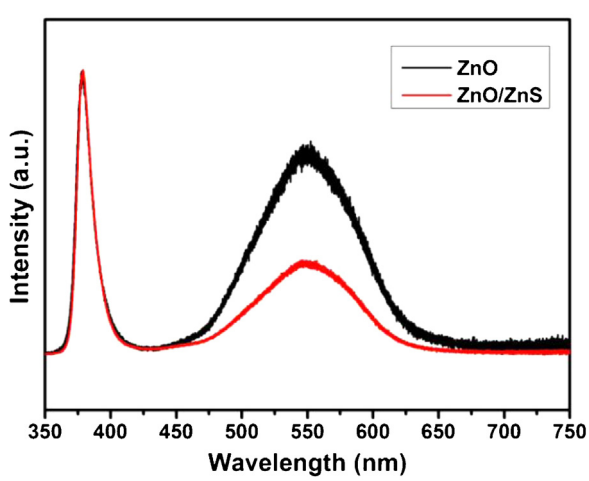

Fig. 4. Room temperature PL spectra of ZnO and ZnO/ZnS structure.

around 550 nm. The UV emission band is ascribed to a near band edge transition of ZnO, which originated from the recombination of the free excitons through an exciton–exciton collision process [21]. The intense emission in the visible region is related to deep-level defects in the ZnO crystal, such as vacancies and interstitials of zinc and oxygen [33,34]. Compared with ZnO NRs, the peak intensity of the deep level emission of the ZnO/ZnS composite nanostructure was much less, which suggested that surface defects were reduced through the formation of a ZnS layer on the ZnO NRs [35,36]. Therefore the charge can transfer from ZnS to ZnO effectively. This is an advantage of depositing a thin ZnS layer on the ZnO NRs for fabricating QDSSCs.

Fig. 5(a) shows the optical absorbance of ZnO/ZnS hierarchical structure and ZnO/ZnS/CdS hierarchical structure with different deposition times of CdS QDs. It can be seen that the ZnO/ZnS nanorod array absorbs in the UV region with a band edge of ~379 nm. After depositing CdS QDs onto ZnO/ZnS nanostructure, the ZnO/ZnS/CdS architecture extends their optical absorptions to the visible region. With increasing the deposition time of CdS QDs, the optical absorption in the visible region is gradually enhanced

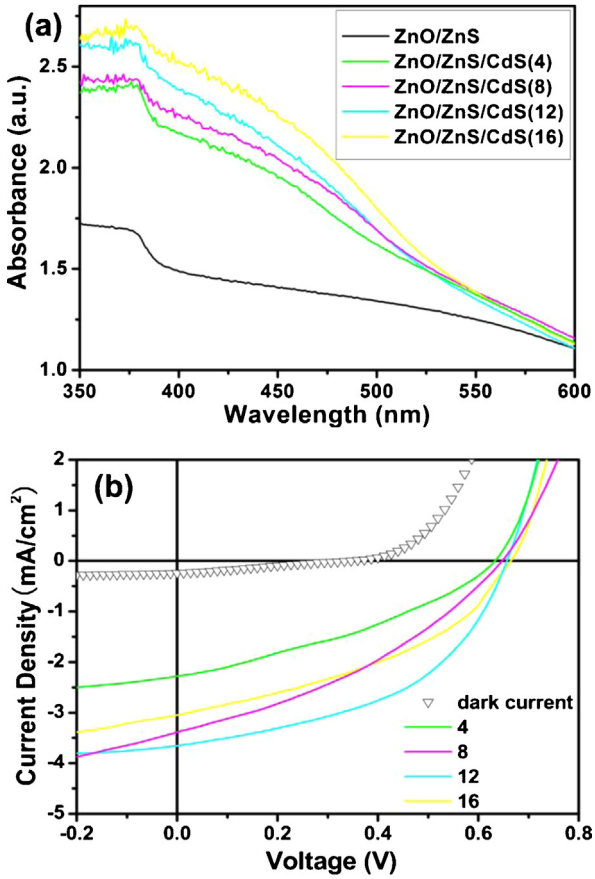

Fig. 5. (a) UV–vis absorption spectra of different electrode and (b) dark current of ZnO/ZnS/CdS(12) and *J–V* characteristic of ZnO/ZnS/CdS electrode with different deposition times of CdS QDs.

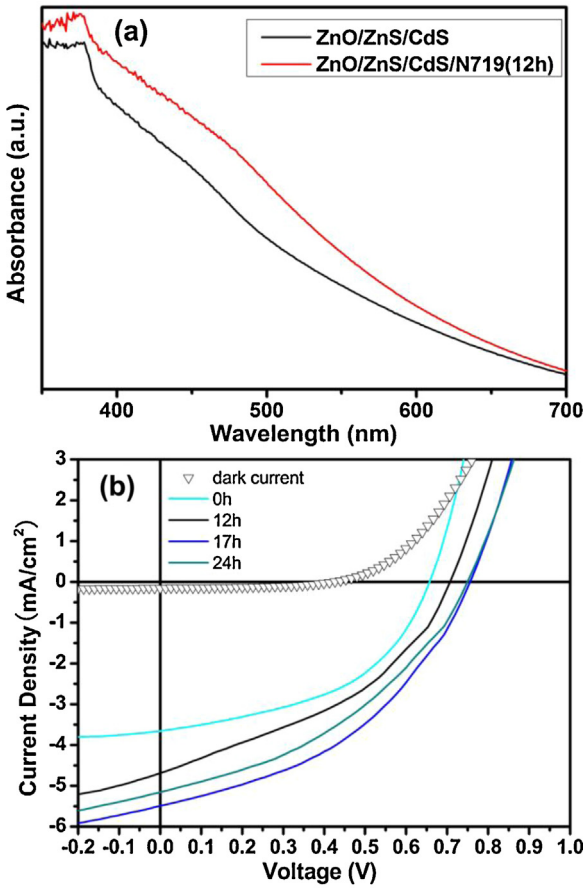

Fig. 6. (a) UV–vis absorption spectra of ZnO/ZnS/CdS electrode with and without N719 (12 h) and (b) dark current of ZnO/ZnS/CdS/N719(17 h) and *J–V* curve of the cosensitized solar cells with different N719 adsorption times.

due to the increased amounts of deposited CdS QDs. This phenomenon was previously encountered in ZnO nanotube-based solar cells by Sun et al. [37]. Thus, we can deduce that photovoltaic properties with our designed CdS-sensitized solar cell based on the ZnO/ZnS core/shell photoanode could be improved by enhancing the optical absorption.

In order to investigate the influence of deposition time for CdS on photovoltaic performance of the ZnO/ZnS/CdS electrodes, current density (*J*)–voltage (*V*) characteristics for CdS-sensitized solar cells based on ZnO/ZnS/CdS(4), ZnO/ZnS/CdS(8), ZnO/ZnS/CdS(12) and ZnO/ZnS/CdS(16) electrodes were measured (4, 8, 12, 16 correspond to SILAR cycle). The results are displayed in Fig. 5(b) and Table 1. With increasing the deposition time of CdS, the energy conversion efficiency (η) of the QDSSCs first increases and then decreases again. The optimized photovoltaic performance with a *Voc* of 0.66 V, a *Jsc* of 3.66 mA/cm^2, an *FF* of 0.48, and a η of 1.16% is obtained from the device based on ZnO/ZnS/CdS(12) electrode. For the device based on ZnO/ZnS/CdS(4) and ZnO/ZnS/CdS(8) electrode, the poor photovoltaic property could be attributed to the thinner CdS NP-layer and the consequent less optical absorption of visible light (as shown in Fig. 5(a)). For the device based on the ZnO/ZnS/CdS(16) electrode, the thicker CdS nanoparticle layer can result in an enhanced optical absorption of visible light (Fig. 5(a)), but it also can increase the recombination chance of photogenerated carriers and then lead to the poor photovoltaic property [9].

To further improve the photovoltaic performance of the QDSSCs with ZnO/ZnS/CdS(12) electrode, a thin layer of N719 dye was deposited onto the ZnO/ZnS/CdS(12) structure. In order to investigate the impact on the photoabsorption of surrounding dye molecules, the optical absorption spectra are tested for ZnO/ZnS/CdS(12) and ZnO/ZnS/CdS(12)/N719 electrodes as shown in Fig. 6(a). After being modified by N719 for 12 h, an enhancement of adsorption spectra in the visible region can be observed, which evidently originates from the adsorption of the dye molecules. However, it does not exactly correspond to the adsorption band of pure N719, which maybe due to the interaction between the dye molecule and the semiconductor surface [37,38]. The *J–V* curve of the cosensitized solar cells with different N719 adsorption time is shown in Fig. 6(b) and the related parameters are listed in Table 2. It is found that the photovoltaic performance of the device can

Table 1
Photovoltaic parameters of QDSSCs based on ZnO/ZnS/CdS electrode with different deposition times of CdS QDs.

CdS	*Jsc* (mA/cm^2)	*Voc* (V)	*FF*	η (%)
4	2.29	0.64	0.37	0.53
8	3.38	0.65	0.36	0.78
12	3.66	0.66	0.48	1.16
16	3.37	0.67	0.41	0.82

Table 2
Photovoltaic parameters of the cosensitized solar cells with different N719 adsorption time.

Time (h)	*Jsc* (mA/cm^2)	*Voc* (V)	*FF*	η (%)
0	3.66	0.66	0.48	1.16
12	4.69	0.70	0.40	1.32
17	5.48	0.75	0.42	1.59
24	5.16	0.75	0.39	1.52

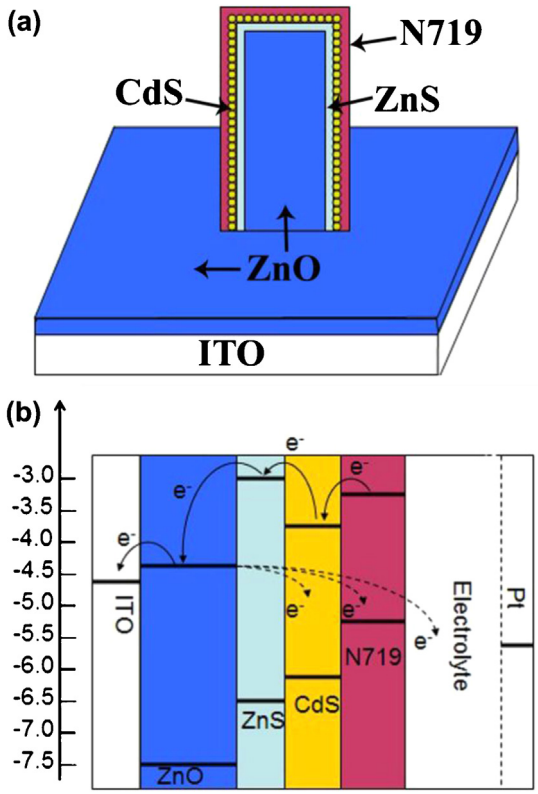

Fig. 7. (a) Schematic configuration for the cosensitized solar cell and (b) charge-transfer process in the solar cell.

be improved by coating the electrode with N719. Sensitized with N719 for 17 h, the device shows a 37% enhancement in energy conversion efficiency compared with the device sensitized only by CdS QDs, displaying a *Voc* of 0.75 V, a *Jsc* of 5.48 mA/cm^2, an *FF* of 0.42, and a η of 1.59%. Although the light absorbance of ZnO/ZnS/CdS/N719(24) is higher in comparison with two other electrodes (ZnO/ZnS/CdS/N719(12) and ZnO/ZnS/CdS/N719(17)), it does not exhibit the best photovoltaic characteristic. This is probably attributed to the dye agglomerates which have been known to be inactive for electron injection and shield the dye molecules in direct contact with CdS from absorbing light [39,40]. It is thus expected that the 24 h-adsorption exhibits lower photocurrent in spite of higher dye loading.

To better understand the mechanism of the improved solar cell efficiency, in Fig. 7, we depicted the main configuration and energy level diagram of the cell after being excited by light. In such a configuration, it can be noticed that the conduction band edge of ZnS is higher than that of ZnO. Thus, the compact ZnS shell is very efficient on retarding the back transfer of electrons and minimizing electron–hole recombination, which significantly decreases the dark current and is beneficial for the final conversion efficiency. In Fig. 7(b), the visible light is absorbed by CdS and N719, and the excited electron–hole pairs are generated. Then, the photogenerated charges in CdS and N719 are effectively separated at the interfaces. Subsequently, driven by the favorable energetic arrangement shown in Fig. 7(b), the separated electrons are efficiently transferred from the CdS shell to the ZnO and then quickly transferred to the ITO substrate along the direct path of the ZnO nanorods. In addition, CdS QDs can nonradiatively transfer energy to N719 through FRET, which is based on long-range dipole–dipole couplings between different chromophores. FRET between two chromophores in photoactive films can improve the photocurrent and overall conversion efficiencies for the designed cosensitized solar cells. Such photocurrent amplifications resulted from funneling excitons toward the heterojunction interfaces, where they split rather than recombine [3,41].

4. Conclusions

In conclusion, ZnO/ZnS core–shell hierarchical structure for use in QDs sensitized solar cells and N719/QDs cosensitized solar cells have been achieved by coating ZnS layer on ZnO NRs using SILAR method. It has been demonstrated that ZnS shell is very efficient on reducing surface defects, retarding the back transfer of electrons and minimizing electron–hole recombination. Through analysis of *J–V* curve, it can be found that the QDSSC based on ZnO/ZnS/CdS(12) architecture showed a maximum power conversion efficiency of 1.16%, which is due to the better light harvesting. By depositing a thin layer of N719 dye onto the ZnO/ZnS/CdS(12) structure can further improve the photovoltaic performance of the solar cells. When ZnO/ZnS/CdS(12) electrode is sensitized with N719 for 17 h, the device shows a 37% enhancement in energy conversion efficiency compared with the device sensitized only CdS QDs, displaying a *Voc* of 0.75 V, a *Jsc* of 5.48 mA/cm^2, an *FF* of 0.42, and a η of 1.59%. In the authors' opinion, the concept of the cosensitization is anticipated to be applicable to other inorganic semiconductor solar cells for future potential applications.

Acknowledgments

The authors acknowledge financial support from National Natural Science Foundation of China (Grant Nos. 11204104, 11254001, 61178074 and 61008051), Program for the Development of Science and Technology of Jilin province (Item Nos. 20110415, 201115219 and 20100113), the Eleventh Five-Year Program for Science and Technology of Education Department of Jilin Province (Item Nos. 20110169 and 20110170), the Open Project Program for National Laboratory of Superhard Materials (No. 201004), Program for the Master Students' Scientific and Innovative Research of Jilin Normal University (Item No. 201112, 201101, 201139).

References

[1] A. Kim, Y. Won, K. Woo, C.H. Kim, J. Moon, Highly transparent low resistance ZnO/Ag nanowire/ZnO composite electrode for thin film solar cells, ACS Nano 7 (2013) 1081, http://dx.doi.org/10.1021/nn305491x.
[2] J.B. Cui, U.J. Gibson, A simple two-step electrodeposition of Cu_2O/ZnO nanopillar solar cells, Journal of Physical Chemistry C 114 (2010) 6408.
[3] M.A. Green, K. Emery, Y. Hishikawa, W. Warta, Solar cell efficiency tables (Version 32), Progress in Photovoltaics: Research and Applications 16 (2008) 435.
[4] B. O'Regan, M. Gratzel, A low-cost, high-efficiency solar cell based on dye-sensitized colloidal TiO_2 films, Nature 353 (1991) 737.
[5] M.K. Nazeeruddin, A. Kay, I. Rodicio, R. Humphry-Baker, E. Muller, P. Liska, N. Valchopoulos, M. Gratzel, Conversion of light to electricity by cis-X2Bis(2,2′-bipyridyl-4,4′-dicarboxylate)ruthenium(II) charge-transfer sensitizers (X = C1–, Br–, I–, CN–, and SCN–) on nanocrystalline TiO_2 electrodes, Journal of the American Chemical Society 115 (1993) 6382.
[6] M. Quintana, T. Edvinsson, A. Hagfeldt, G. Boschloo, Comparison of dye-sensitized ZnO and TiO_2 solar cells: studies of charge transport and carrier lifetime, Journal of Physical Chemistry C 111 (2007) 1035.
[7] T. Ganesh, R.S. Mane, G. Cai, J.H. Chang, S.H. Han, ZnO nanoparticles–CdS quantum dots/N_3 dye molecules: dual photosensitization, Journal of Physical Chemistry C 113 (2009) 7666.
[8] P.V. Kamat, Quantum dot solar cells: semiconductor nanocrystals as light harvesters, Journal of Physical Chemistry C 112 (2008) 18737.
[9] B. Sun, Y.Z. Hao, F. Guo, Y.H. Cao, Y.H. Zhang, Y.P. Li, D.S. Xu, Fabrication of Poly(3-hexylthiophene)/CdS/ZnO core–shell nanotube array for semiconductor-sensitized solar cell, Journal of Physical Chemistry C 116 (2012) 1395.
[10] M. Shalom, J. Albero, Z. Tachan, E. Martínez-Ferrero, A. Zaban, E. Palomares, Quantum dot–dye bilayer-sensitized solar cells: breaking the limits imposed by the low absorbance of dye monolayers, Journal of Physical Chemistry Letters 1 (2010) 1134.
[11] K. Shankar, X.J. Feng, C.A. Grimes, Enhanced harvesting of red photons in nanowire solar cells: evidence of resonance energy transfer, ACS Nano 3 (2009) 788.

[12] Y.Q. Liu, J. Wang, Co-sensitization of TiO_2 by PbS quantum dots and dye N719 in dye-sensitized solar cells, Thin Solid Films 518 (2010) e54.
[13] S. Buhbut, S. Itzhakov, E. Tauber, M. Shalom, I. Hod, T. Geiger, Y. Garini, D. Oron, A. Zaban, Built-in quantum dot antennas in dye-sensitized solar cells, ACS Nano 4 (2010) 1293.
[14] M.J. Currie, J.K. Mapel, T.D. Heidel, S. Goffri, M.A. Baldo, High-efficiency organic solar concentrators for photovoltaics, Science 321 (2008) 226.
[15] M.A. Baldo, D.F. O'Brien, Y. You, A. Shoustikov, S. Sibley, M.E. Thompson, S.R. Forrest, Highly efficient phosphorescent emission from organic electroluminescent devices, Nature 395 (1998) 151.
[16] P.T.K. Chin, R.A.M. Hikmet, R.A.J. Janssen, Energy transfer in hybrid quantum dot light-emitting diodes, Journal of Applied Physics 104 (2008) 013108.
[17] L. Etgar, J. Park, C. Barolo, V. Lesnyak, S.K. Panda, P. Quagliotto, S.G. Hickey, M.K. Nazeeruddin, A. Eychmüller, G. Viscardib, M. Grätzela, Enhancing the efficiency of a dye sensitized solar cell due to the energy transfer between CdSe quantum dots and a designed squaraine dye, RSC Advances 2 (2012) 2748.
[18] Y.F. Sun, J.H. Yang, L.L. Yang, J. Cao, M. Gao, Z.Q. Zhang, Z. Wang, H. Song, Improve the open-circuit voltage of ZnO solar cells with inserting ZnS layers by two ways, Journal of Solid State Chemistry 200 (2013) 258.
[19] Q.X. Zhao, L.L. Yang, M. Willander, B.E. Sernelius, P.O. Holtz, Surface recombination in ZnO nanorods grown by chemical bath deposition, Journal of Applied Physics 104 (2008) 073526.
[20] R. Yousefi, A.K. Zak, M.R. Mahmoudian, Growth and characterization of Cl-doped ZnO hexagonal nanodisks, Journal of Solid State Chemistry 184 (2011) 2678.
[21] Y.F. Sun, J.H. Yang, L.L. Yang, M. Gao, X.N. Shan, Z.Q. Zhang, M.B. Wei, Y. Liu, L.H. Fei, H. Song, Less contribution of nonradiative recombination in ZnO nails compared with rods, Journal of Luminescence 134 (2013) 35.
[22] Z. Gu, M.P. Paranthaman, J. Xu, Z.W. Pan, Aligned ZnO nanorod arrays grown directly on zinc foils and zinc spheres by a low-temperature oxidization method, ACS Nano 3 (2009) 273.
[23] C. Li, G.J. Fang, J. Li, L. Ai, B.Z. Dong, X.Z. Zhao, Effect of seed layer on structural properties of ZnO nanorod arrays grown by vapor-phase transport, Journal of Physical Chemistry C 112 (2008) 990.
[24] K. Wang, J.J. Chen, Z.M. Zeng, J. Tarr, W.L. Zhou, Y. Zhang, Y.F. Yan, C.S. Jiang, J. Pern, A. Mascarenhas, Synthesis and photovoltaic effect of vertically aligned ZnO/ZnS core/shell nanowire arrays, Applied Physics Letters 96 (2010) 123105.
[25] A. Umar, Y.B. Hahn, Ultraviolet-emitting ZnO nanostructures on steel alloy substrates: growth and properties, Crystal Growth and Design 8 (2008) 2741.
[26] X. Fan, M.L. Zhang, I. Shafiq, W.J. Zhang, C.S. Lee, S.T. Lee, ZnS/ZnO heterojunction nanoribbons, Advanced Materials 21 (2009) 2393.
[27] S.A. Vanalakar, S.S. Mali, R.C. Pawar, N.L. Tarwal, A.V. Moholkar, J.H. Kim, P.S. Patil, Photoelectrochemical properties of CdS sensitized ZnO nanorod arrays: effect of nanorod length, Journal of Applied Physics 112 (2012) 044302.
[28] B. Vincent Crist, Handbook of Monochromatic XPS Spectra: The Elements and Native Oxides, John Wiley & Sons, England, 2000, 510 pp.
[29] L.L. Yang, Q.X. Zhao, M. Willander, X.J. Liu, M. Fahlman, J.H. Yang, Effective suppression of surface recombination in ZnO nanorods arrays during the growth process, Crystal Growth and Design 10 (2010) 1904.
[30] Y.F. Lu, H.Q. Ni, Z.H. Mai, Z.M. Ren, The effects of thermal annealing on ZnO thin films grown by pulsed laser deposition, Journal of Applied Physics 88 (2000) 498.
[31] H.H. Wang, S.H. Baek, J.J. Song, J.H. Lee, S.W. Lim, Microstructural and optical characteristics of solution-grown Ga-doped ZnO nanorod arrays, Nanotechnology 19 (2008) 075607.
[32] J. Cao, J.H. Yang, L.L. Yang, M.B. Wei, B. Feng, D.L. Han, L. Fan, B.J. Wang, H. Fu, The effects of doping and shell thickness on the optical and magnetic properties of Mn/Cu/Fe-doped and Co-doped ZnS nanowires/ZnO quantum dots/SiO2 heterostructures, Journal of Applied Physics 112 (2012) 014316.
[33] C. Ronning, P. Gao, X.Y. Ding, Z.L. Wang, D. Schwen, Manganese-doped ZnO nanobelts for spintronics, Applied Physics Letters 84 (2004) 783.
[34] P. Yang, H.Q. Yan, S. Mao, R. Russo, J. Johnson, R. Saykally, N. Morris, J. Pham, R. He, H.J. Choi, Controlled growth of ZnO nanowires and their optical properties, Advanced Functional Materials 12 (2002) 323.
[35] J. Chung, J. Myoung, J. Oh, S. Lim, Synthesis of a ZnS shell on the ZnO nanowire and its effect on the nanowire-based dye-sensitized solar cells, Journal of Physical Chemistry C 114 (2010) 21360.
[36] B.D. Yao, Y.F. Chen, N. Wang, Formation of ZnO nanostructures by a simple way of thermal evaporation, Applied Physics Letters 81 (2002) 757.
[37] J. Luo, C.M. Liu, S.H. Yang, Y. Cao, Hybrid solar cells based on blends of poly(3-hexylthiophene) and surface dye-modified, ultrathin linear- and branched-TiO_2 nanorods, Solar Energy Materials and Solar Cells 94 (2010) 501.
[38] Y.F. Zhang, H.R. Zhang, Y.F. Wang, W.F. Zhang, Efficient visible spectrum sensitization of $BaSnO_3$ nanoparticles with N719, Journal of Physical Chemistry C 112 (2008) 8553.
[39] C.R. Lee, H.S. Kim, I.H. Jang, J.H. Im, N.G. Park, Pseudo first-order adsorption kinetics of N719 dye on TiO_2 surface, ACS Applied Materials & Interfaces 3 (2011) 1953.
[40] K. Keis, J. Lindgren, S.E. Lindquist, A. Hagfeldt, Studies of the adsorption process of Ru complexes in nanoporous ZnO electrodes, Langmuir 16 (2000) 4688.
[41] A. Ruland, C. Schulz-Drost, V. Sgobba, D.M. Guldi, Enhancing photocurrent efficiencies by resonance energy transfer in CdTe quantum dot multilayers: towards rainbow solar cells, Advanced Materials 23 (2011) 4573.